




Article

Magnetic Field Effect on Thermal, Dielectric, and Viscous Properties of a Transformer Oil-Based Magnetic Nanofluid [†]

Michal Rajnak ^{1,2,*} , Zan Wu ³, Bystrik Dolnik ², Katarina Paulovicova ¹, Jana Tothova ² , Roman Cimbala ², Juraj Kurimský ² , Peter Kopcansky ¹, Bengt Sunden ³ , Lars Wadsö ⁴  and Milan Timko ^{1,*}

¹ Institute of Experimental Physics SAS, Watsonova 47, 04001 Kosice, Slovakia; paulovic@saske.sk (K.P.); kopcan@saske.sk (P.K.)

² Faculty of Electrical Engineering and Informatics, Technical University of Kosice, Letna 9, 04200 Kosice, Slovakia; bystrik.dolnik@tuke.sk (B.D.); jana.tothova@tuke.sk (J.T.); roman.cimbala@tuke.sk (R.C.); juraj.kurimsky@tuke.sk (J.K.)

³ Department of Energy Sciences, Lund University, 22100 Lund, Sweden; Zan.Wu@energy.lth.se (Z.W.); Bengt.Sunden@energy.lth.se (B.S.)

⁴ Division of Building Materials, Lund University, 22100 Lund, Sweden; lars.wadso@byggtek.lth.se

* Correspondence: rajnak@saske.sk (M.R.); timko@saske.sk (M.T.)

[†] This paper is an extended version of our paper published in Conference proceedings of 1st International Conference on Nanofluids (ICNf2019), ISBN eBook en PDF: 978-84-685-3917-1, pp. 95–98.

Received: 30 October 2019; Accepted: 25 November 2019; Published: 28 November 2019



Abstract: Progress in electrical engineering puts a greater demand on the cooling and insulating properties of liquid media, such as transformer oils. To enhance their performance, researchers develop various nanofluids based on transformer oils. In this study, we focus on novel commercial transformer oil and a magnetic nanofluid containing iron oxide nanoparticles. Three key properties are experimentally investigated in this paper. Thermal conductivity was studied by a transient plane source method dependent on the magnetic volume fraction and external magnetic field. It is shown that the classical effective medium theory, such as the Maxwell model, fails to explain the obtained results. We highlight the importance of the magnetic field distribution and the location of the thermal conductivity sensor in the analysis of the anisotropic thermal conductivity. Dielectric permittivity of the magnetic nanofluid, dependent on electric field frequency and magnetic volume fraction, was measured by an LCR meter. The measurements were carried out in thin sample cells yielding unusual magneto-dielectric anisotropy, which was dependent on the magnetic volume fraction. Finally, the viscosity of the studied magnetic fluid was experimentally studied by means of a rheometer with a magneto-rheological device. The measurements proved the magneto-viscous effect, which intensifies with increasing magnetic volume fraction.

Keywords: magnetic nanofluid; magnetic nanoparticles; thermal conductivity; viscosity; permittivity

1. Introduction

Electrical equipment, like power transformers, inherently operate with energy losses, which lead to rises in temperature. To prevent premature aging and the ultimate failure of the equipment, the heat generated through energy loss must be dissipated. In practice, this is usually achieved by circulating transformer oils (TO), which also ensures the electrical insulation of energized conductors [1]. However, with the development of the future high-voltage network and smart grid, the increasing requirement for reliability and performance of dielectric and cooling liquids motivates researchers to develop more

effective liquid media using nanotechnology [2]. Thus, various nanofluids have been synthesized with the aim of improving the cooling and insulating properties of the base dielectric liquid. Besides the conventional nanoparticles, such as TiO_2 or Al_2O_3 , these improvements have been achieved also with graphene nanosheets [3,4], fullerene [5], or magnetic nanoparticles (MNPs) [6,7]. The stable dispersions of MNPs in TO (well-known as magnetic nanofluids or ferrofluids) have an advantage over other nanofluids due to the controllability of thermal, dielectric, and viscous properties by an external magnetic field. Like in other nanofluids, the addition of MNPs to TO causes an increase in viscosity and this is a drawback for pumping power. However, the phenomenon of thermomagnetic convection [8–10] and the possibility of controlling nanofluid flow by the external magnetic field makes magnetic nanofluids (MNFs) attractive and suitable candidates for the replacement of TO.

With regards to the potential application of transformer oil-based MNFs in power transformers, most research studies have focused on three key properties: thermal, dielectric, and viscous. Within the study of thermal properties, the thermal conductivity of MNFs attracts scientific interest, in addition to research on thermomagnetic convection. In comparison to TO, the thermal conductivity of MNFs is increased due to the presence of MNPs. This is often interpreted by means of various static and dynamic mechanisms and models used for nanofluids in general [11]. On the other hand, this property is a function of the base liquid, dispersed particles, size distribution, volume fraction, surfactant, and the external magnetic field. The influence of listed factors on the thermal conductivity of MNFs has been documented in numerous papers, some of them reviewed in a recent review article [12]. From the literature, one can see that the thermal conductivity of MNFs is generally enhanced in the presence of a magnetic field regardless of the MNF type. However, some of the studies report huge increments in thermal conductivity [13–15], while others refer to smaller increments, with the applied magnetic field [16,17]. These differences are also found for similar types of MNF samples and similar measurement setups used. One can assume that these discrepancies may originate in MNF characterization or in the differences in magnetic field distribution acting on studied MNFs. Generally, it was shown that such discrepancies might also arise due to nanoparticle aggregation [18]. It is well-known that under an external magnetic field, the nanoparticles in an MNF can exhibit self-assembly and micromotion [19]. Structural changes are initiated by moments of force causing the rotation of the nanoparticles that are parallel with the field. The interparticle magnetic forces can then lead to the formation of chain-like clusters [20]. Due to the formed heterogeneous structure in MNF, the thermal conductivity is anisotropic. It was found that the thermal conductivities parallel to the magnetic field direction are, in most cases, much higher than the perpendicular ones [21–23]. Thus, the magnetic field direction and distribution in the study of MNF thermal conductivity plays a key role.

The insulating and dielectric properties of TO were found to exhibit peculiar enhancement upon the addition of MNPs [23–27]. A comprehensive mechanism of the increased breakdown field strength is still unknown, however, a few models have been proposed. In the nanoparticle charging model [28], the difference in the dielectric permittivity of the dispersed nanoparticles and the surrounding oil is considered as an essential condition leading to polarization, charge trapping, and subsequent reduction of streamer velocity. Thus, the dielectric permittivity of MNF is a crucial parameter that has been extensively studied [29–31]. Again, the effect of an external magnetic field and the induced heterogeneous nanoparticle structure results in magneto-dielectric anisotropy [32]. This is mostly characterized by higher dielectric permittivity measured in the parallel configuration of electric and magnetic fields as compared to perpendicular configuration. Furthermore, the magnetic field induced MNP assembly also results in the well-known magneto-viscous effect. This effect is expressed as the ratio between the viscosity increment under the field and the viscosity value in the absence of the field and it reaches a maximum for a critical MNP size [33]. There are numerous studies demonstrating that the viscosity of MNFs is dependent on the flow shear rate, nanoparticle volume fraction, temperature, magnetic field, or MNP interaction [34–36]. Recently, an empirical correlation was proposed to predict magneto-viscous behavior of MNFs, as a function of these parameters [37].

In this study, we investigate the three key quantities of an MNF based on a novel, commercially available TO. Taking into account the referenced discrepancies in the thermal conductivity data in the literature, we intend to present other seemingly counter-intuitive experimental results. We discuss that the discrepancies may result from the way the magnetic field is applied and distributed through the MNF sample volume with regards to the measuring sensor. Similarly, we report on the unusual magneto-dielectric anisotropy and complement the study with the measurements of the viscosity of the MNF dependent on the magnetic field and magnetic volume fraction.

2. Materials and Methods

The investigated MNF is based on a commercially available inhibited insulating transformer oil MOL TO 40A. Its basic physical properties provided by the manufacturer are as follows: density 0.867 g/cm^3 , kinematic viscosity $22 \text{ mm}^2/\text{s}$, pour point 228 K , flash point 413 K , and interfacial tension 42 mN/m . The dispersive phase consists of superparamagnetic iron oxide nanoparticles, which are coprecipitated from ferrous and ferric ions in an aqueous solution according to this well-known procedure [38]. To stabilize the MNP in the TO, we used oleic acid as a surfactant. The stabilized MNPs are dispersed in the TO in the following solid volume fraction 0.39%, 0.97%, 1.39%, 1.92%, and 3.62% with the corresponding physical parameters presented in Table 1. These samples have been stable for 2 years.

Table 1. The basic physical parameters of the prepared magnetic nanofluid samples.

| Sample | Magnetization of Saturation (kA/m) | Magnetic Volume Fraction (%) | DC Magnetic Susceptibility (-) | Density (g/cm^3) | Solid Volume Fraction (%) |
|------------|------------------------------------|------------------------------|--------------------------------|-----------------------------|---------------------------|
| MOL TO 40A | - | - | - | 0.867 | 0 |
| MNF_MOL 1 | 1.68 | 0.377 | 0.05 | 0.884 | 0.39 |
| MNF_MOL 2 | 3.598 | 0.807 | 0.11 | 0.909 | 0.97 |
| MNF_MOL 3 | 5.223 | 1.171 | 0.15 | 0.927 | 1.39 |
| MNF_MOL 4 | 7.469 | 1.675 | 0.21 | 0.95 | 1.92 |
| MNF_MOL 5 | 9.802 | 2.198 | 0.24 | 1.023 | 3.62 |

The solid volume fraction is calculated according to the following formula: $\varphi = (\rho_{\text{MNF}} - \rho_{\text{TO}}) / (\rho_{\text{MNP}} - \rho_{\text{TO}})$, where ρ_{MNF} , ρ_{TO} , and ρ_{MNP} are the densities of the MNF, TO, and MNP, respectively. The density of magnetite (5.18 g/cm^3) was substituted in ρ_{MNP} . The magnetic volume fraction is determined as a ratio of the MNF magnetization of saturation to the domain magnetization of magnetite (446 kA/m) [39]. The magnetic properties of the MNF samples were measured by means of a vibrating sample magnetometer installed on a cryogen-free superconducting magnet from Cryogenic Limited. The obtained magnetization curves measured at 298 K in the field ranging up to 6 T are shown in Figure 1. The mean particle size derived from the fitting of the magnetization curve by the superposition of Langevin functions is 11.1 nm . From Figure 1, one can observe the typical superparamagnetic behavior with zero coercivity and remanence. At higher magnetic fields (above 2 T), the magnetization is well saturated and increases with the increasing magnetic volume fraction.

The measurements of thermal conductivity were carried out by a thermal constant analyzer (TPS 2500S, Hot Disk AB, Sweden) using a transient plane source method (TPS). The spiral sensor with the axial and radial probing depth of 1.2 mm was inserted vertically into a Teflon container filled with the probed MNF. The diameter of the sensor is 3.2 mm . Figure 2 shows a schematic illustration and a real picture of the double Hot Disk sensor and its assembly with the Teflon sample container.

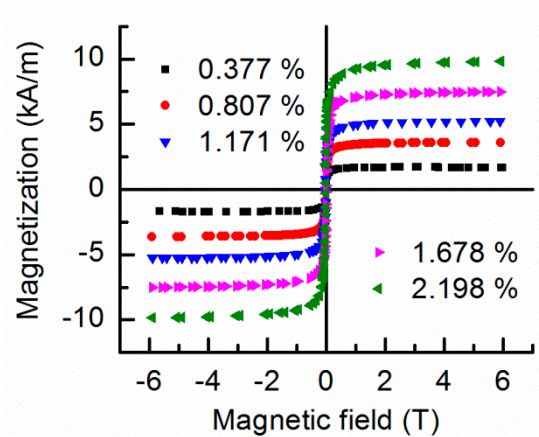


Figure 1. Magnetization curves of magnetic nanofluid samples with various magnetic volume fractions. The measurements were performed at a temperature of 298 K.

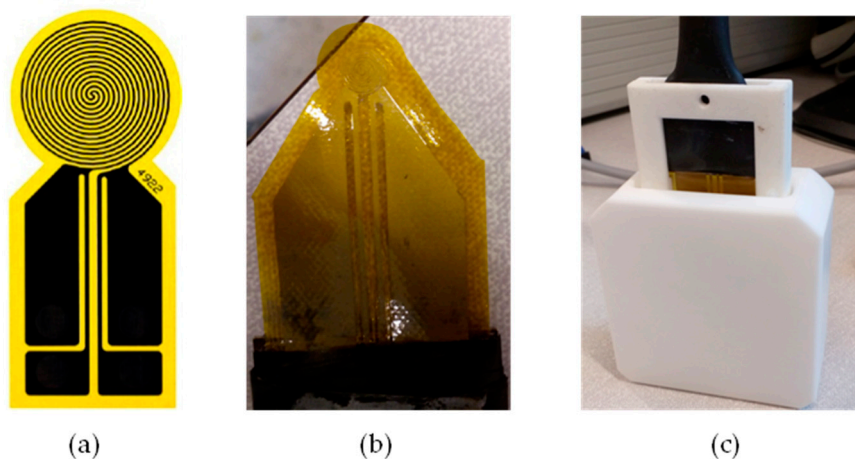


Figure 2. A schematic illustration of the double spiral Hot Disk sensor (a). The picture of the sensor with Kapton insulation (b). The sensor fixed in a Teflon frame inserted in the sample container (c).

The static magnetic field acting on the investigated MNF samples was generated between a pair of permanent magnets (37 mm apart) attached to the walls of the sample container (Figure 3a). With various sets of permanent magnets, the average magnetic field of 45 mT, 90 mT, and 210 mT in the sensor location was proven by a Hall probe. The particular magnetic field value was changed by manual attachment of the prepared magnetic set. Further experimental tests confirmed the unmeasurable effect of the present magnetic field on the Hot Disk sensor. In Figure 3b, we present a schematic arrangement of the permanent magnets with the simulated distribution of the magnetic flux density. A more detailed color pattern of magnetic flux density simulated in the sample area between the two strongest magnets is demonstrated in Figure 3c,d.

The numerical simulation of the magnetic flux density near the permanent magnets was simulated by Finite Element Method Magnetics (FEMM 4.2) using the triangular element mesh and the iterative conjugate solver. We changed the default mesh density to a finer mesh density, 1 mm for the air, and 0.25 mm for the permanent magnet. The electrical and magnetic parameters of the Neodymium Iron Boron permanent magnet was set as follows: the relative permeability $\mu_r = 1.049$, the coercivity $H_c = 1.13$ MA/m, and the electrical conductivity $\sigma = 0.667$ MS/m. The distribution of magnetic flux density and the isolines of magnetic flux density between the two permanent magnets was achieved by using the GNU Octave high-level language, version 4.0.0. Using this type of magnetic field distribution simulation supports subsequent analysis of the magnetic field dependent thermal conductivity of magnetic fluids.

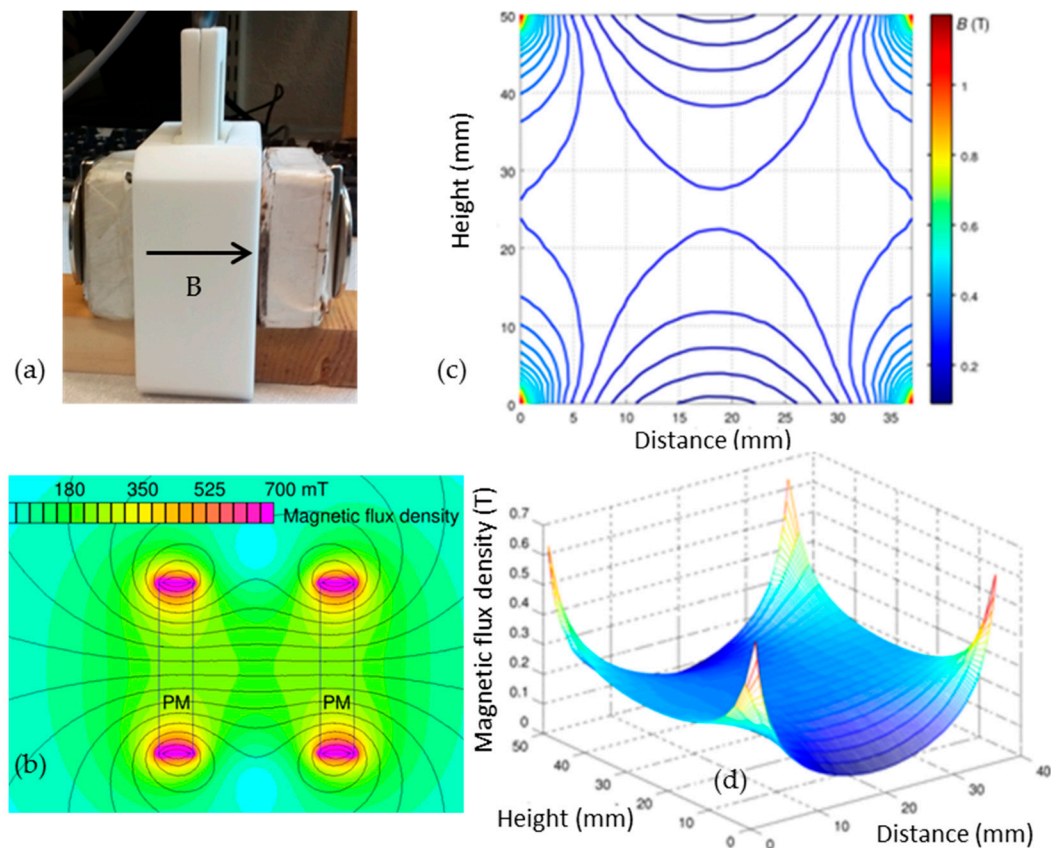


Figure 3. Set of permanent magnets attached to the Teflon sample container (a). Simulation of magnetic flux density distribution around the permanent magnets (PM) (b). More detailed color flux density plots for the sample area between the two strongest magnets applied in the experiment (c,d).

The frequency-dependent dielectric permittivity of the studied MNF was measured in commercial liquid crystal cells. The sandwiched type cells are composed of two flat glass pieces coated with indium tin oxide (ITO) conductive layers acting as electrodes. The electrodes are $50\ \mu\text{m}$ apart while the active electrode area is $25\ (5 \times 5)\ \text{mm}^2$. Firstly, the capacity of the empty cells C_0 was measured, yielding the value $7.5\ \text{pF}$. Then, the cells were filled with investigated TO and MNF samples. To study the magnetic field effect, the sample cell was placed between two poles of an electromagnet. The dielectric spectroscopy measurements were carried out at room temperature using an LCR meter (Agilent E4980A) with the effective voltage value across the capacitor of $1\ \text{V}$.

The viscous properties of the MNF samples under a magnetic field were studied by using an Anton Paar rheometer MCR 502 with the magneto-rheological device (MRD). MRD is a special accessory of the MCR rheometer, which enables all rheological tests with the simultaneous action of the external magnetic field.

3. Results and Discussion

3.1. Thermal Conductivity

In Figure 4a, we present the dependence of the thermal conductivity (TC) of the MNF on the magnetic volume fraction in the absence of the external magnetic field. The TC of the pure TO was found to be $0.127\ \text{W/mK}$. It is clearly shown that with the addition of MNP, the TC increases moderately. The lowest magnetic volume fraction 0.377% results in a 3.9% increase in TC, while for the highest magnetic volume fraction of 2.198% , the TC of MNF increases by 9.2% , compared to the pure TO. Clearly, the thermal conductivity increases with the magnetic volume fraction because the particle

thermal conductivity is higher than that of the oil. Higher thermal conductivity of the particles indicates a lower temperature drop across the particles. In this way, various approaches could be chosen to model the experimentally well-known increase in TC with increasing MNP volume fraction. In the simple approach, taking into account the non-interacting spherical MNPs of low concentration, one can apply an effective medium theory, such as the Maxwell model described by Equation [11],

$$k_{\text{eff}} = \frac{k_p + 2k_f + 2\Phi(k_p - k_f)}{k_p + 2k_f - \Phi(k_p - k_f)} k_f, \quad (1)$$

where k and Φ denote the thermal conductivity and the solid volume fraction of the MNP. The subscripts eff, p, and f indicate the nanofluid, the particle, and the base fluid (TO), respectively. The substitution of particular values (for magnetite nanoparticles $k_p = 1.39$ W/mK is considered) yields k_{eff} of 0.29 W/mK and 1.24 W/mK for magnetic volume fractions equal to 0.377% and 0.807%, respectively. These values are higher than those measured in the experiments. Moreover, for higher MNP volume fractions, the relation yields negative values of k_{eff} . Thus, the Maxwell model is not sufficient to explain the observed thermal conductivity in the MNF. More sophisticated models with an emphasis on the interfacial thermal resistance (Kapitza resistance), the nanoscale layer between the TO and MNPs, or the nanoconvection induced by the Brownian motion of MNPs should be considered in a future study. The development of such a model is beyond the scope of this work.

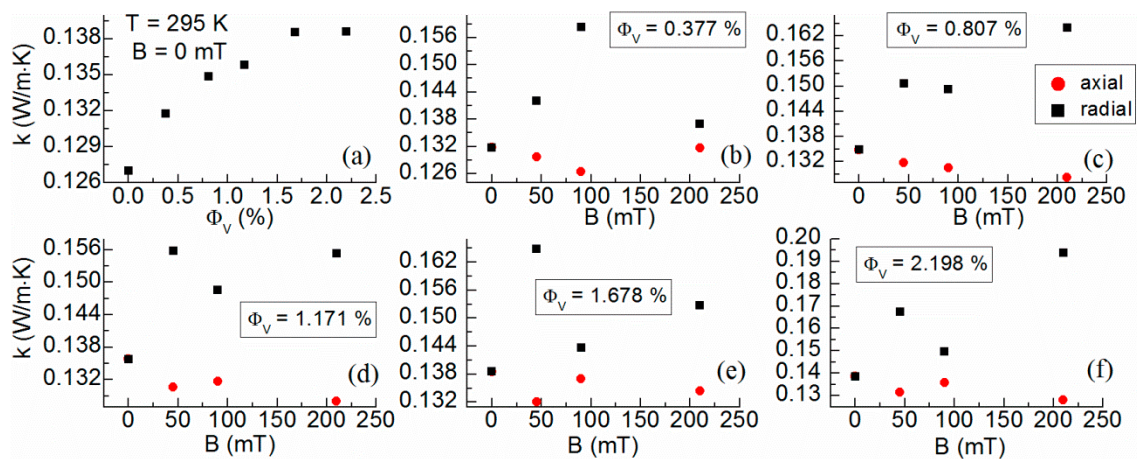


Figure 4. Dependence of the magnetic nanofluid (MNF) thermal conductivity on the magnetic volume fraction (a). The effect of the magnetic field on the thermal conductivity of the MNF of various magnetic volume fractions probed in the axial and radial directions of the Hot Disk sensor (b–f).

From Figure 4b–f, one can observe the changes of TC with an increasing magnetic field for particular MNF samples. These measurements were conducted in an anisotropic mode. First of all, when comparing the two components of TC, each MNF sample exhibits a higher TC in the radial direction (perpendicular to the magnetic field intensity), compared to the axial one (parallel with the magnetic field intensity). This is observed for each magnetic field value. The finding is partly in contradiction to the previous studies, which mostly report an opposite anisotropic effect. Usually, a higher TC in a parallel direction to the applied magnetic field is associated with MNP interaction with the field and the subsequent aggregation of MNP. However, one has to bear in mind that in these experiments, not only the magnetic field direction and intensity affect the aggregation and the TC of MNF, but the magnetic field gradient ∇B has a determining character too. In a homogenous magnetic field with $\nabla B = 0$, the nanoparticles do not experience any drag force. Nevertheless, the magnetic moments orientate (Brownian or Néel mechanism) with the field, and a chain-like structure may be formed. Such MNP structures locally form rapid heat conduction paths (percolation paths), and so

along the paths, the TC is increased. The enhanced TC due to the formed aggregation has been proven numerically for nanofluids in general [40,41]. However, in a strong gradient magnetic field the formed MNP structures can weaken, break, and drag in the field gradient. It is very important to know the exact magnetic field distribution with regard to the sensor location in the MNF. From our simulations of the magnetic flux density in Figure 3, we can clearly observe denser contours of the magnetic field near the edges of the magnets. The increasing magnetic flux density towards the container edges are also illustrated in the color scale. The simulation, therefore, proves that the MNF in the experimental container experiences a gradient magnetic field, which exerts a drag force on the MNPs. As a result, instead of horizontal chain structures, the nanoparticles are forced to form aggregates directed to the edges of the container. Now, realizing that the thin Hot Disk sensor is located in the center of the container, it is clear that in the axial (horizontal) probing depth, the MNF contains fewer MNPs (decreased effective magnetic volume fraction) due to the above-mentioned reasoning. This is reflected in lower axial TC detected for each magnetic field value. On the other hand, the aggregates formed from the center towards the container edges constitute the increased heat conduction paths and contribute to the higher radial TC, as revealed in the experiment. However, in Figure 4b–f, we do not observe a strictly proportional increase of the radial TC with an increasing magnetic field. The data exhibits a rather stochastic behavior. In our opinion, this is attributed to a different re-distribution of MNPs at a new magnetic field value. As mentioned in Section 2, the new magnetic field value is achieved by attaching a new set of permanent magnets manually. Clearly, the manual attachment of the opposing magnets might not be exactly symmetric with regards to the Hot Disk sensor, and each set of magnets may lead to slightly different distributions of the MNP aggregates. Nevertheless, for each magnet set and the related magnetic field value, we have proven a higher radial TC in comparison to its axial part.

3.2. Dielectric Permittivity

From a dielectric point of view, we focus on the dielectric response of the studied MNF and present the dielectric permittivity measured from 700 Hz up to 100 kHz. This frequency range is chosen deliberately to observe magneto-dielectric anisotropy in MNFs that are free of pronounced interfacial polarization, conductivity and space charge migration, and electrode polarization, which has been documented, for example, in the paper with the reference number [42]. The resulting dielectric spectra for the three MNF samples are plotted in Figure 5.

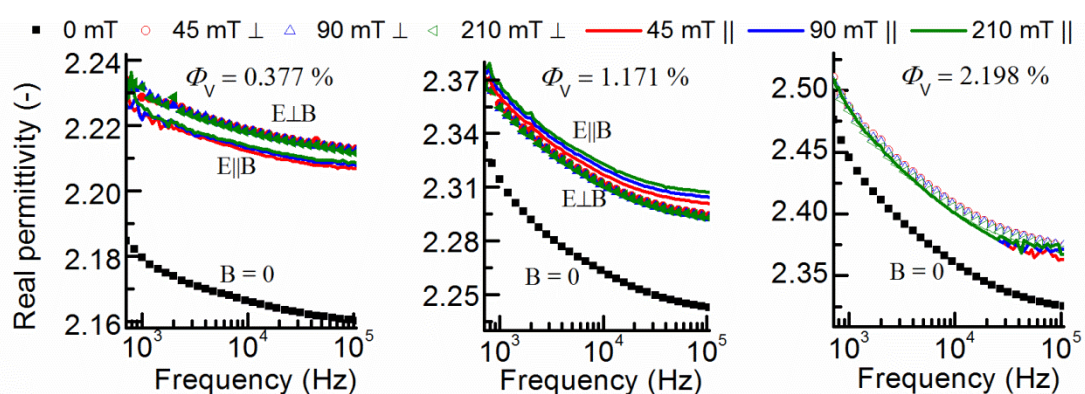


Figure 5. The spectra of real dielectric permittivity of magnetic nanofluids with various magnetic volume fractions. The graphs show the effect of the magnetic fields and their orientation with regards to measuring the electric field. The measurements were performed at room temperature.

The dielectric permittivity of the pure TO at 1 kHz is 2.12, and this value has been found to be quasi constant in the whole frequency range. The addition of MNP with the volume fraction of 0.377%, 1.171%, and 2.198% results in the permittivity values of 2.18, 2.31, and 2.45, respectively. Thus, at 1 kHz, these relatively low MNP volume fractions do not increase the oil's permittivity to a great

extent. However, the spectrum of the permittivity is markedly shifted to higher values upon the application of the magnetic field, as demonstrated in the graphs of Figure 5. This effect is associated with MNP assembly in the field direction. For the sample of a higher magnetic volume fraction (2.198%), we do not observe any magneto-dielectric anisotropy, as the permittivity values measured in the parallel configuration of electric and magnetic field intensities coincide with those measured in the perpendicular configuration. This behavior is ascribed to measuring capacitor geometry (50 μm electrode separation distance, 25 mm^2 electrode area) and close packing of the MNP aggregates. In contrast to the gradient magnetic field in the previous case, in this experiment the magnetic field in the active sample volume is homogenous. It is believed that even though the MNP chains are oriented in the magnetic field direction, their relative distances are so close that the lateral or transversal polarization of the chain assembly in the MNF yields an equivalent dielectric response. A slight difference in perpendicular and parallel permittivity is observed at the lower magnetic volume fraction (1.171%). In this case, the slightly higher parallel permittivity is attributed to the prevailing charge accumulation at the chain terminals (head and tail), which are close to the electrodes. However, for the lowest MNP volume fraction, the two configurations of the fields give the opposite anisotropic effect. Clearly, for perpendicular configuration, the permittivity is slightly higher than the one measured in the parallel configuration. This may reflect in such a structural chain arrangement, in which the transversal polarization of the chains results in a higher bound charge formation in the capacitor than with the one associated with the polarization along the chains. This could happen in the thin MNF sample, with the chains separated from each other enough. Finally, it may be concluded from Figure 5 that the observable permittivity change appears under the action of the 45 mT magnetic field, while the higher field values do not induce further changes in the permittivity of such a thin MNF sample.

3.3. Viscosity

The TO involved in this study exhibits Newtonian behavior with a dynamic viscosity of 15.7 mPa. With the dispersed MNPs of magnetic volume fractions 0.377%, 0.807%, 1.171%, 1.678%, and 2.198%, the viscosity increases to values of 16.53 mPa, 16.76 mPa, 17.3 mPa, 18.31 mPa, and 19.3 mPa, respectively, (at a temperature of 294 K) and also behaves as a Newtonian fluid. The well-known magneto-viscous effect is observed in the presence of the external magnetic field. This is presented in the dynamic viscosity vs. shear rate graphs (flow curves) for the three selected MNF samples in Figure 6.

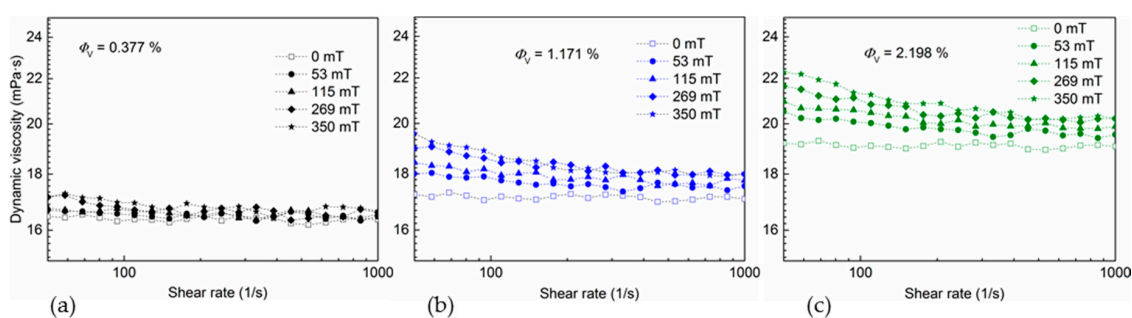


Figure 6. The flow curves under the external magnetic field of various magnitudes plotted for the samples with magnetic volume fractions of 0.377% (a), 1.171% (b), and 2.198% (c).

In Figure 6a, a weak magneto-viscous effect is observed. Even though a quite strong magnetic field (350 mT) is acting on the low-concentrated MNF, the magneto-viscous effect does not arise markedly. This is attributed to the low MNP concentration in which the probability of greater MNP chain formation in the shear flow is low. However, from Figure 6b,c one can see the increasing magneto-viscous effect with the increasing magnetic field. This phenomenon is associated with the magnetic and mechanic torques, which hinder the free rotation of MNPs and their chains in the shear flow. Here, one should realize that the magnetic field is oriented perpendicular to the vorticity of the

shear flow. The perpendicular orientation of the MNP chains, which are composed of a small fraction of larger MNPs in the MNF, then leads to an increase in the dynamic viscosity, especially at low shear rates. However, at higher shear rates, the MNP chains disrupt due to intensive fluid flow and this gives rise to the observed shear thinning. Thus, the non-Newtonian behavior with a shear-thinning effect is confirmed for this MNF. The shear-thinning and the magneto-viscous effect become stronger with increasing magnetic volume fraction. A more detailed description of the mechanism and condition leading to the magneto-viscous effect may be found in reference [43].

4. Conclusions

The measurements of thermal conductivity of the transformer oil-based magnetic nanofluid revealed a moderate increase in thermal conductivity with increasing magnetic volume fraction. In the presence of the external magnetic field, a remarkable anisotropy in thermal conductivity was found. The apparently strange anisotropy was discussed in consideration of the magnetic field gradient around the thermal conductivity sensor. The arrangement of the magnetic nanoparticle aggregates in the magnetic field gradient is a decisive factor determining the local thermal conductivity in the magnetic nanofluid. Dielectric spectroscopy measurements of the magnetic nanofluid in the thin sample cell revealed the magnetodielectric anisotropy dependent on the magnetic volume fraction. The studied nanofluid exhibits non-Newtonian behavior with the remarkable shear thinning in the external magnetic field. Based on the obtained results one can conclude that the increased thermal conductivity, low dielectric permittivity, and viscosity make the studied magnetic nanofluid suitable for further testing in real electrical equipment, such as power transformers.

Thus, the investigated parameters of the magnetic nanofluid depend on the magnetic field and the related nanoparticle suspension, aggregate state, or morphology within the bulk liquid. However, the applied experimental methods in this study do not allow one to see the aggregate or agglomeration morphology. Moreover, the three measurement techniques do not use the equivalent magnetic field distributions and sample geometry. This limitation complicates the linking of the three parameters together in a reliable empirical correlation. On the other hand, fitting correlations for these properties would require further comprehensive investigation at various temperatures. Therefore, the presented results might challenge other researchers to carry out simultaneous (in situ) measurements of a particular parameter investigated in this study and the structural properties, e.g., by means of in situ scattering techniques.

Author Contributions: M.R. conceived the study, contributed to the dielectric, magnetic, and thermal measurements and analysis, and wrote the paper. Z.W., B.S. and L.W. designed and carried out the thermal conductivity measurements, B.D. performed the simulations of the magnetic field distribution, and J.K. and R.C. designed the dielectric spectroscopy experiments; K.P. was responsible for the sample preparation and J.T. designed and carried out the measurements of viscosity. P.K. and M.T. were responsible for the resources, formal analysis, and presentation of the study.

Funding: This research was funded by the Slovak Academy of Sciences and Ministry of Education in the framework of the projects: VEGA 2/0141/16, 1/0250/18 and 1/0340/18; the Slovak Research and Development Agency under the Contract Number APVV-18-0160 and APVV-15-0438; the Ministry of Education Agency for structural funds of EU Project ITMS 313011T565, ERANET FMF, ERANET MAGBRRIS and Cultural and Educational Grant Agency of the Ministry of Education, Science, Research and Sport of the Slovak Republic (KEGA) under the project No. 008TUKE-4/2019. APC was funded by Nanouptake COST Action (European Cooperation in Science and Technology), www.cost.eu.

Acknowledgments: This article is based upon work from COST Action Nanouptake, supported by COST (European Cooperation in Science and Technology) www.cost.eu. The study is the result of Nanouptake STSM accomplished by Michal Rajnak and Zan Wu. Zan Wu, Milan Timko, and Peter Kopcansky acknowledge the COST Action Nanouptake for financial support in the participation of the 1st International Conference on Nanofluids (ICNf) and the 2nd European Symposium on Nanofluids (ESNf).

Conflicts of Interest: The authors declare no conflict of interest.

References

1. Fofana, I. 50 years in the development of insulating liquids. *IEEE Electr. Insul. Mag.* **2013**, *29*, 13–25. [[CrossRef](#)]

2. Wang, X.; Tang, C.; Huang, B.; Hao, J.; Chen, G. Review of research progress on the electrical properties and modification of mineral insulating oils used in power transformers. *Energies* **2018**, *11*, 487. [[CrossRef](#)]
3. Bhunia, M.M.; Panigrahi, K.; Das, S.; Chattopadhyay, K.K.; Chattopadhyay, P. Amorphous graphene—Transformer oil nanofluids with superior thermal and insulating properties. *Carbon* **2018**, *139*, 1010–1019. [[CrossRef](#)]
4. Sen Gupta, S.; Manoj Siva, V.; Krishnan, S.; Sreeprasad, T.S.; Singh, P.K.; Pradeep, T.; Das, S.K. Thermal conductivity enhancement of nanofluids containing graphene nanosheets. *J. Appl. Phys.* **2011**, *110*, 084302. [[CrossRef](#)]
5. Chen, J.; Sun, P.; Sima, W.; Shao, Q.; Ye, L.; Li, C. A promising nano-insulating-oil for industrial application: Electrical properties and modification mechanism. *Nanomaterials* **2019**, *9*, 788. [[CrossRef](#)] [[PubMed](#)]
6. Pislaru-Danescu, L.; Morega, A.M.; Telipan, G.; Morega, M.; Dumitru, J.B.; Marinescu, V. Magnetic nanofluid applications in electrical engineering. *IEEE Trans. Magn.* **2013**, *49*, 5489–5497. [[CrossRef](#)]
7. Rajnak, M.; Timko, M.; Kopcansky, P.; Paulovicova, K.; Kuchta, J.; Franko, M.; Kurimsky, J.; Dolnik, B.; Cimbala, R. Transformer oil-based magnetic nanofluid with high dielectric losses tested for cooling of a model transformer. *IEEE Trans. Dielectr. Electr. Insul.* **2019**, *26*, 1343–1349. [[CrossRef](#)]
8. Nkurikiyimfura, I.; Wang, Y.; Pan, Z. Heat transfer enhancement by magnetic nanofluids—A review. *Renew. Sustain. Energy Rev.* **2013**, *21*, 548–561. [[CrossRef](#)]
9. Lee, M.; Kim, Y.-J. Thermomagnetic Convection of Ferrofluid in an Enclosure Channel with an Internal Magnetic Field. *Micromachines* **2019**, *10*, 553. [[CrossRef](#)]
10. Vatani, A.; Woodfield, P.L.; Nguyen, N.T.; Dao, D.V. Onset of thermomagnetic convection around a vertically oriented hot-wire in ferrofluid. *J. Magn. Magn. Mater.* **2018**, *456*, 300–306. [[CrossRef](#)]
11. Bianco, V.; Manca, O.; Nardini, S.; Vafai, K. *Heat Transfer Enhancement with Nanofluids*; CRC Press: Boca Raton, FL, USA, 2015; ISBN 1482254026.
12. Doganay, S.; Alsangur, R.; Turgut, A. Effect of external magnetic field on thermal conductivity and viscosity of magnetic nanofluids: A review. *Mater. Res. Express* **2019**, *6*, 112003. [[CrossRef](#)]
13. Patel, J.; Parekh, K.; Upadhyay, R.V. Maneuvering thermal conductivity of magnetic nanofluids by tunable magnetic fields. *J. Appl. Phys.* **2015**, *117*, 243906. [[CrossRef](#)]
14. Philip, J.; Shima, P.D.; Raj, B. Enhancement of thermal conductivity in magnetite based nanofluid due to chainlike structures. *Appl. Phys. Lett.* **2007**, *91*, 203108.
15. Shima, P.D.; Philip, J.; Raj, B. Magnetically controllable nanofluid with tunable thermal conductivity and viscosity. *Appl. Phys. Lett.* **2009**, *95*, 133112. [[CrossRef](#)]
16. Altan, C.L.; Elkatmis, A.; Yüksel, M.; Aslan, N.; Bucak, S. Enhancement of thermal conductivity upon application of magnetic field to Fe₃O₄ nanofluids. *J. Appl. Phys.* **2011**, *110*, 093917.
17. Parekh, K.; Lee, H.S. Magnetic field induced enhancement in thermal conductivity of magnetite nanofluid. *J. Appl. Phys.* **2010**, *107*, 09A310.
18. Wu, Z.; Sundén, B. Convective heat transfer performance of aggregate-laden nanofluids. *Int. J. Heat Mass Transf.* **2016**, *93*, 1107–1115. [[CrossRef](#)]
19. Odenbach, S. *Colloidal Magnetic Fluids: Basics, Development and Application of Ferrofluids*; Springer: Berlin, Germany, 2009; ISBN 9783540853862.
20. Jin, J.; Song, D.; Geng, J.; Jing, D. Time-dependent scattering of incident light of various wavelengths in ferrofluids under external magnetic field. *J. Magn. Magn. Mater.* **2018**, *447*, 124–133. [[CrossRef](#)]
21. Gavili, A.; Zabihi, F.; Isfahani, T.D.; Sabbaghzadeh, J. The thermal conductivity of water base ferrofluids under magnetic field. *Exp. Therm. Fluid Sci.* **2012**, *41*, 94–98. [[CrossRef](#)]
22. Katiyar, A.; Dhar, P.; Nandi, T.; Das, S.K. Magnetic field induced augmented thermal conduction phenomenon in magneto-nanocolloids. *J. Magn. Magn. Mater.* **2016**, *419*, 588–599. [[CrossRef](#)]
23. Li, Q.; Xuan, Y.; Wang, J. Experimental investigations on transport properties of magnetic fluids. *Exp. Therm. Fluid Sci.* **2005**, *30*, 109–116. [[CrossRef](#)]
24. Segal, V.; Hjortsberg, A.; Rabinovich, A.; Natrass, D.; Raj, K. AC (60 Hz) and impulse breakdown strength of a colloidal fluid based on transformer oil and magnetite nanoparticles. In Proceedings of the Conference Record of the 1998 IEEE International Symposium on Electrical Insulation (Cat. No.98CH36239), Arlington, VA, USA, 7–10 June 1998; Volume 2, pp. 619–622.
25. Lee, J.-C.; Seo, H.-S.; Kim, Y.-J. The increased dielectric breakdown voltage of transformer oil-based nanofluids by an external magnetic field. *Int. J. Therm. Sci.* **2012**, *62*, 29–33. [[CrossRef](#)]
26. Kurimský, J.; Rajňák, M.; Cimbala, R.; Rajnič, J.; Timko, M.; Kopčanský, P. Effect of magnetic nanoparticles on partial discharges in transformer oil. *J. Magn. Magn. Mater.* **2019**, *496*, 165923. [[CrossRef](#)]

27. Kurimský, J.; Rajňák, M.; Bartko, P.; Paulovičová, K.; Cimbala, R.; Medved, D.; Džamová, M.; Timko, M.; Kopčanský, P. Experimental study of AC breakdown strength in ferrofluid during thermal aging. *J. Magn. Magn. Mater.* **2018**, *465*, 136–142. [[CrossRef](#)]
28. Hwang, J.G.; Zahn, M.; O'Sullivan, F.M.; Pettersson, L.A.A.; Hjortstam, O.; Liu, R. Effects of nanoparticle charging on streamer development in transformer oil-based nanofluids. *J. Appl. Phys.* **2010**, *107*, 014310. [[CrossRef](#)]
29. Rajnak, M.; Spitalsky, Z.; Dolnik, B.; Kurimsky, J.; Tomco, L.; Cimbala, R.; Kopcansky, P.; Timko, M. Toward Apparent Negative Permittivity Measurement in a Magnetic Nanofluid with Electrically Induced Clusters. *Phys. Rev. Appl.* **2019**, *11*, 024032. [[CrossRef](#)]
30. Rajnak, M.; Kurimsky, J.; Dolnik, B.; Kopcansky, P.; Tomasovicova, N.; Taculescu-Moaca, E.A.; Timko, M. Dielectric-spectroscopy approach to ferrofluid nanoparticle clustering induced by an external electric field. *Phys. Rev. E* **2014**, *90*, 032310. [[CrossRef](#)]
31. Malaescu, I.; Marin, C.N. Dependence on the temperature of the activation energy in the dielectric relaxation processes for ferrofluids in low-frequency field. *J. Magn. Magn. Mater.* **2002**, *252*, 68–70. [[CrossRef](#)]
32. Spanoudaki, A.; Pelster, R. Frequency dependence of dielectric anisotropy in ferrofluids. *J. Magn. Magn. Mater.* **2002**, *252*, 71–73. [[CrossRef](#)]
33. Shahrivar, K.; Morillas, J.R.; Luengo, Y.; Gavilan, H.; Morales, P.; Bierwisch, C.; de Vicente, J. Rheological behavior of magnetic colloids in the borderline between ferrofluids and magnetorheological fluids. *J. Rheol.* **2019**, *63*, 547–558. [[CrossRef](#)]
34. Rosa, A.P.; Cunha, F.R. The influence of dipolar particle interactions on the magnetization and the rotational viscosity of ferrofluids. *Phys. Fluids* **2019**, *31*, 052006. [[CrossRef](#)]
35. Susan-Resiga, D.; Socoliuc, V.; Boros, T.; Borbáth, T.; Marinica, O.; Han, A.; Vékás, L. The influence of particle clustering on the rheological properties of highly concentrated magnetic nanofluids. *J. Colloid Interface Sci.* **2012**, *373*, 110–115. [[CrossRef](#)] [[PubMed](#)]
36. Odenbach, S.; Pop, L.M.; Zubarev, A.Y. Rheological properties of magnetic fluids and their microstructural background. *GAMM Mitt.* **2007**, *30*, 195–204. [[CrossRef](#)]
37. Shojaeizadeh, E.; Veysi, F.; Goudarzi, K.; Feyzi, M. Magnetoviscous effect investigation of water based Mn-ZnFe₂O₄ magnetic nanofluid under the influence of magnetic field: An experimental study. *J. Magn. Magn. Mater.* **2019**, *477*, 292–306. [[CrossRef](#)]
38. Vékás, L.; Bica, D.; Avdeev, M.V. Magnetic nanoparticles and concentrated magnetic nanofluids: Synthesis, properties and some applications. *China Particuol.* **2007**, *5*, 43–49. [[CrossRef](#)]
39. Rosensweig, R.E. *Ferrohydrodynamics*; Dover Publications: New York, NY, USA, 2013; ISBN 0486783006.
40. Prasher, R.; Evans, W.; Meakin, P.; Fish, J.; Phelan, P.; Keblinski, P. Effect of aggregation on thermal conduction in colloidal nanofluids. *Appl. Phys. Lett.* **2006**, *89*, 143119. [[CrossRef](#)]
41. Evans, W.; Prasher, R.; Fish, J.; Meakin, P.; Phelan, P.; Keblinski, P. Effect of aggregation and interfacial thermal resistance on thermal conductivity of nanocomposites and colloidal nanofluids. *Int. J. Heat Mass Transf.* **2008**, *51*, 1431–1438. [[CrossRef](#)]
42. Rajnak, M.; Dolnik, B.; Kurimsky, J.; Cimbala, R.; Kopcansky, P.; Timko, M. Electrode polarization and unusual magnetodielectric effect in a transformer oil-based magnetic nanofluid thin layer. *J. Chem. Phys.* **2017**, *146*, 014704. [[CrossRef](#)]
43. Odenbach, S.; Thurm, S. Magnetoviscous Effects in Ferrofluids. In *Ferrofluids*; Springer: Berlin/Heidelberg, Germany, 2002; pp. 185–201.

